Identifiability Analysis of Planar Rigid-Body Frictional Contact

Identifiability Analysis of Planar Rigid-Body Frictional Contact

Nima Fazeli, Russ Tedrake and Alberto Rodriguez

Abstract This paper addresses the identifiability of the inertial parameters and the contact forces associated with an object making and breaking frictional contact with the environment. Our goal is to explore under what conditions, and to what degree, the observation of physical interaction, in the form of motions and/or forces, is indicative of the underlying dynamics that governs it. In this initial study we consider the cases of passive interaction, where an object free-falls under gravity, and active interaction, where known external perturbations act on the object at contact. We assume that both object and environment are planar and rigid, and exploit the well-known complementarity formulation for contact resolution to establish a closed-form relationship between inertial parameters, contact forces, and observed motions. Consistent with intuition, the analysis indicates that without the application of known external forces, the identifiable set of parameters remains coupled, i.e., the ratio of mass moment of inertia to mass and the ratio of contact forces to the mass. Interestingly, the analysis also shows that known external forces can lead to decoupling and identifiability of mass, mass moment of inertia, and normal and tangential contact forces. We evaluate the identifiability formulation both in simulation and with real experiments.

1 Introduction

Autonomous manipulation in an uncertain environment requires an autonomous understanding of contact. *A priori* models of objects and their environment are routinely deficient or defective: In some cases it is not cost-effective to build accurate models; others the complex and ever-transforming nature of nature renders it im-

Nima Fazeli and Alberto Rodriguez
Mechanical Engineering Department, MIT, USA e-mail: <nfazeli,albertor>@mit.edu

Russ Tedrake
Computer Science and Artificial Intelligence Laboratory, MIT, USA e-mail: russt@csail.mit.edu

possible. This understanding of contact is often implicit in the design of a manipulator. By carefully choosing materials and geometries we can passively deal with uncertainty. However, when we want to monitor or actively control the execution of a manipulation task, an explicit understanding of the algebra between motions, forces, and inertias at contact is principal.

We are inspired by human's unconscious but effective ability to make sense of contact to understand its environment. It only takes us a small push to a cup of coffee to estimate how full it is, and a quick glance to a bouncing ball to gauge its stiffness. This work builds on the conviction that, similarly, robots can harness known laws of physical interaction to make sense of observed motions and/or forces, and as a result gain a better understanding of their environment and themselves.

In particular, in this initial study we explore the identifiability of inertial parameters and contact forces associated with planar frictional contact interactions. We exploit the linear complementarity formulation (LCP) of contact resolution [18, 1] to relate inertial parameters, contact forces, and observed motions. Section 3 reviews the structure of an LCP problem and describes the mathematical framework necessary to outline the identifiability analysis.

The specific system we consider is a single planar rigid body undergoing impact after a period of free fall, as in Fig. 1. What can we say about an object from observing its motions and/or forces? The falling trajectory is a simple ballistic motion, which can be fitted to the dynamics of free fall. The key challenge, and focus of this paper, is in finding a formulation suitable for system identification, that can handle the complexity of unknown and spurious reaction forces due to frictional contact. Such a formulation might yield a systematic approach for a broader set of contact interactions including sliding, pushing or grasping.

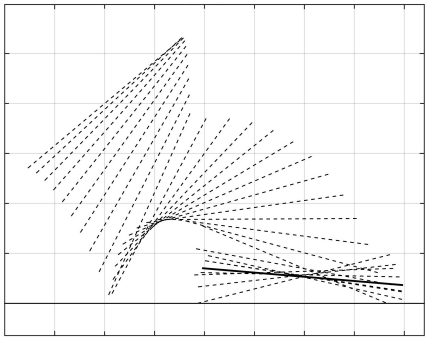

Fig. 1: Stewart and Trinkle [18] used the example of a falling rod to introduce a time-stepping complementarity scheme for contact resolution that has become one of the standard techniques for simulating frictional contact. In this paper we look at the same formulation and similar examples from the perspective of identification. Is the trajectory of the rod indicative enough of the dynamic system that governs its motion?

Our main contribution is a systematic analysis of the question of the identifiability of the mass, the moment of inertia, and contact forces from kinematic observations of frictional contact interactions. Section 4 details the analysis both for cases when contacts stick or slip, as well as when known external forces are applied during contact.

In this paper we use a batch approach to system identification, where we extract the best possible inertial parameters and contact forces that explain a series of observations. A potential benefit over more traditional calibration methods for parameter fitting, is that equivalent on-line techniques are well understood and readily available. Section 5 evaluates the validity of the approach analysis with simulated and real experiments with a planar block and a planar ellipse falling on a flat ground, which are captured with a high-speed camera.

2 Background & Motivation

System identification studies the problem of fitting a model (i.e., inertial parameters) to a series of inputs (i.e., forces and torques) and responses (i.e., displacements/velocities/accelerations) of a dynamic system. The most basic idea behind system identification is that, although the response of a dynamic system tends to be complex, the governing dynamics are often linear in a set of observable parameters. For example, while $\sum \mathbf{f} = m \cdot \mathbf{a}$ can lead to complex trajectories, forces and accelerations are still linearly related by m. This allows closed-form least-squares formulations for the estimation of those parameters.

System ID is the process of identifying what parameters are instrumental and what observations are informative, and then make estimates of the parameters from measured data. This idea has been applied in robotics to the identification of serial and parallel link manipulators [7, 8], and to identify inertial parameters sufficient for control purposes [17].

In this paper we show that system identification has the potential to provide a formal approach to observe rigid-body contact interactions, which, in turn, opens with a wide set of possible applications: Contact-aware state estimation (Erdmann [6], Atkeson [3], Koval et al [9], Zhang and Trinkle [22], Trinkle [20], Yu et al [21]); Contact-aware planning and control (Lynch and Mason [10], Platt and Kaelbling [12], Posa et al [13], Chavan Dafle and Rodriguez [5]); Fault detection or task monitoring (Rodriguez et al [15], Salawu [16]).

One of the main assumptions in our approach is the selection of a time-stepping Linear Complementarity Problem (LCP) scheme for the resolution of forces and accelerations during frictional contact. Why LCP? Brogliato et al [4] identifies 3 classes of methods for rigid body simulation:

i. *Penalty methods* model interaction as a reaction force proportional to the amount of interpenetration. Although easier to solve, they lack in realism.
ii. *Event-driven methods* rely on a listing, resolution, and selection of all possible contact/impact events. They typically require some knowledge of contact time.

Müller and Pöschel [11] showed that they can lead to exceedingly high velocities in situations with multiple contacts.

iii. *Time-stepping methods* integrate the equations of motion during a finite time interval. Should a contact (or multiple) be detected during the interval, the algorithm resolves the collisions and continues to integrate the equations of motion.

The time-stepping approach, in conjunction with the velocity-impulse resolution of contact, which results in a Complementarity Problem (CP), has been advocated by Stewart and Trinkle [18] and Anitescu and Potra [2] among others, and has been shown to be robust to phenomena such as Painleve's problem [19], and always to have a solution, with linear approximations of the friction cone and for a positive definite mass matrix.

3 Complementarity Problems for Collision Resolution

The standard approach to resolve motion, which we sometimes refer to as Euler integration, follows the simple iterative scheme:

$$\text{Current state} \longrightarrow \begin{array}{c}\text{Compute resultant}\\ \text{of applied forces}\end{array} \longrightarrow \begin{array}{c}\text{Integrate forward}\\ \text{to next state}\end{array} \tag{1}$$

One of the core difficulties in dealing with contact is that it breaks that basic scheme. The motion of the system depends on the resultant of applied forces, but at the same time these applied forces (friction and contact normal) depend on the motion of the system. As a consequence, both contact forces and resulting motions must be determined (searched for) simultaneously, instead of sequentially as in (1).

This section reviews the complementarity formulation for contact resolution which solves simultaneously for contact forces and velocities. For further details we refer the reader to Stewart [19].

A Linear Complementarity Problem

A general (i.e. nonlinear) complementarity problem is defined as:

$$\text{Find: } z \qquad \text{s.t.} \qquad 0 \leq g(z), \qquad 0 \leq z, \qquad 0 = z \cdot g(z) \tag{2}$$

A linear complementarity problem is formed when g is of the form $g(z) = Mz + q$. The benefit of a complementarity formulation is that it allows us to write the equations of motion of a dynamic system with contact defined as unilateral constraints (and that mathematicians have devised solvers for that kind of problem). Force balance looks like:

$$M(q)\frac{dv}{dt} = J_n c_n + D(q)c_t + k(q,v) - \nabla V(q) + F_{ext}(t) \tag{3}$$

where:

- $J_n c_n(t)$ and $D(q)c_t(t)$ represent the normal and tangential contact forces;
- $J_n = \nabla \phi_n(q)$, is the gradient of a function $\phi_n(q)$ that determines the boundary between no contact ($\phi_n(q) > 0$) and penetration ($\phi_n(q) < 0$);
- $D(q)$ is a set of column vectors that linearly span the tangent space at contact, and the product $D(q)c_t$ represents the actual frictional force at a contact;
- $V(q)$ represents conservative forces, such as gravity;
- $k(q,v)$ represents the centrifugal and Coriolis velocity components;
- and F_{ext} represents all external non-conservative forces excluding contact.

The motion at contact, and the tangential contact forces due to friction are related by the principle of maximal dissipation [1] which states that during contact the selection of both has to maximize dissipation, i.e., generally that friction tends to oppose motion:

$$\min_{c_t} (v^+)^T D(q) c_t \qquad \text{such that: } \psi(c_t) \leq \mu c_n \tag{4}$$

Contact resolution then will need to search for the components of c_t such that the frictional force $D(q)c_t$ opposes velocity, from within a valid domain of frictional forces $\psi(c_t) \leq \mu c_n$. If we follow Coulomb's law, all possible frictional forces must lie inside a cone $FC(q) = \{D(q)c_t \text{ s.t. } ||c_t||^2 \leq \mu c_n\}$, where now $\psi(c_t) = ||c_t||^2$. In general, ψ can be shown to be convex, coercive and positively homogeneous which implies that $D(q)c_t \in c_n FC(q)$ is equivalent to $\psi(c_t) \leq \mu c_n$.

We can convert (4) into a CP constraint by noting that the inequality constraint can be incorporated in the minimization by using a Lagrange multiplier $h(c_t, \lambda) = (v^+)^T D(q)c_t - \lambda(\mu c_n - \psi(c_t))$ where now the condition for minimum is:

$$\frac{\partial h}{\partial c_t} = \mu D(q)^T v^+ + \lambda \frac{\partial \psi(c_t)}{\partial c_t} = 0 \tag{5}$$

Furthermore we can write:

$$\begin{aligned} &0 \in \mu D(q)^T v^+ + \lambda \frac{\partial \psi(c_t)}{\partial \psi} \\ &0 \leq \lambda, \qquad 0 \leq \mu c_n - \psi(c_t), \qquad 0 = \lambda(\mu c_n - \psi(c_t)) \end{aligned} \tag{6}$$

which completes the CP formulation for contact resolution:

$$\begin{aligned} \frac{dq}{dt} = vM(q)\frac{dv}{dt} &= J_n c_n + D(q)c_t - \nabla V(q) + k(q,v) + F_{ext} \\ &\text{s.t. } 0 \leq c_n \perp 0 \leq \phi_n, \ 0 \in \mu D(q)^T v^+ + \lambda \frac{\partial \psi(c_t)}{\partial \psi} \\ &\text{s.t. } 0 \leq \lambda \perp 0 \leq \mu c_n - \psi(c_t), \ 0 = J_n^T v^+ \text{ if } \phi_n(q) = 0 \end{aligned} \tag{7}$$

Note that the formulation so far is nonlinear with respect to the friction surface constraint (ψ). For the sake of resolution, it is common linearize the CP by approximating ψ as a polyhedral convex cone. We construct it by using a finer discretization

of the tangent plane at contact with a set of vectors $\{J_n + \mu d_i(q) | i = 1,2,...,m\}$ that positively span it. It is convenient to chose these vectors equiangular with respect to each other, and are paired as $d_i = -d_j$, which we stack in a new matrix $\tilde{D}(q)$. Now we can express the friction force as $\tilde{D}(q)\tilde{c}_t$ where $\tilde{c}_t \geq 0$ and $\Sigma \tilde{c}_{ti} \leq \mu c_n$. Note that we will drop the tilde from the notation but in the rest of the paper, we will assume that the polyhedral approximation holds for all further analysis.

Finally, the CP formulation for contact resolution is:

$$\begin{aligned} q_{k+1} &= q_k + h \cdot v_{k+1} \\ M(q_k)(v_{k+1} - v_k) &= c_n J_n(q_k) + D(q_k)c_t - h \cdot k(q_k, v_k) - h \cdot \nabla V(q_k) + h \cdot F_{\text{ext}} \\ 0 \leq c_n \perp 0 &\leq J_n(q_k)^T (v_{k+1} + \varepsilon v_k) \\ 0 \leq c_t \perp 0 &\leq \lambda e + D(q_k)^T v_{k+1} \\ 0 \leq \lambda \perp 0 &\leq \mu c_n - e^T c_t \end{aligned} \tag{8}$$

A Time-Stepping Approach

Next, to be able to simulate the evolution of the dynamics we convert the formulation to its time-stepping equivalent, for which we integrate the contact forces over a time step. The resulting equations of motion and constraints follow Stewart [19]. We integrate the expressions in (8) forward in time using an Euler scheme. Distance to contact is captured by a measure of the closest distance between boundary of two rigid bodies:

$$\Phi = \begin{bmatrix} \phi_n & \phi_t \end{bmatrix}^T \tag{9}$$

where $\phi_n > 0$ signals free space, $\phi_n = 0$ contact, and $\phi_n < 0$ interpenetration. Fig. 2 depicts an arbitrary planar rigid body with active contact constraints:

$$\Phi = \begin{bmatrix} \phi_n \\ \phi_t \end{bmatrix} = \begin{bmatrix} y - l(\beta)\cos(\beta - \theta) \\ x - l(\beta)\sin(\beta - \theta) \end{bmatrix} = \begin{bmatrix} 0 \\ 0 \end{bmatrix} \tag{10}$$

where angle β parameterizes the object boundary and localizes the contact point. It is a function of θ such that $0 \leq \beta(\theta) < 2\pi$. We compute the Jacobian of the constraint for the equation of motion (3) as:

$$\frac{\partial \Phi}{\partial q} = \begin{bmatrix} J_n \\ J_t \end{bmatrix} = \begin{bmatrix} 0 & 1 & J_y(\theta) \\ 1 & 0 & J_x(\theta) \end{bmatrix} \tag{11}$$

where the rows of $\frac{\partial \Phi}{\partial q}$ can be seen as contact forces, and:

$$\begin{aligned} J_y &= -\frac{\partial \beta}{\partial \theta}\left(\frac{\partial l}{\partial \beta}\cos(\beta - \theta) - l\sin(\beta - \theta)\right) - l\sin(\beta - \theta) \\ J_x &= -\frac{\partial \beta}{\partial \theta}\left(\frac{\partial l}{\partial \beta}\sin(\beta - \theta) + l\cos(\beta - \theta)\right) + l\cos(\beta - \theta) \end{aligned} \tag{12}$$

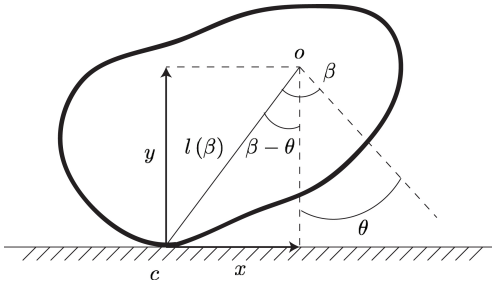

Fig. 2: 2D Rigid Body in Contact

In general, this formulation gives us the contact mode post-impact given pre-impact kinematic measurements, and externally applied forces. On the other hand, if the contact-mode is known, then there is no need to solve the CP. Impulses during impact and velocities/positions post-impact can be solved strictly as functions of these states and external influences pre-impact. We use this fact in Section 4.1 and Section 4.2 to find close form relations between forces, accelerations, and inertial parameters.

4 Identifiability Analysis

In this section we study the identifiability of the inertial parameters (mass and second moment of inertia) and contact forces of a rigid body as it comes into contact with a rigid and fixed flat surface. We assume that the positions, orientations and velocities (linear and angular) of the object are given and the external forces acting on the object are known. The second moment of inertia of the object is expressed with respect to a reference frame attached to the center of mass. Given that kinematic measurements of the trajectory are available, we can derive the direction of friction by invoking the principle of maximum dissipation as outlined in Section 3. We will denote the direction by J_t. We consider sticking and sliding contact modes separately in the following subsections.

4.1 Sliding Contact Mode

During sliding the complementarity constraints from (8) become:

$$0 < c_n, \qquad 0 < c_t, \qquad 0 < \lambda \tag{13}$$

The first inequality derives from the fact that at contact the distance constraint is equal to zero so its dual must be greater than zero. To understand the second and

third inequalities we point out that since we have sliding contact then v_{k+1} must have at least one component that is not perpendicular to the tangent plane spanned by D and so $\max -d_i v_{k+1} \leq \lambda$ where d_i are the columns of D. This directly implies that $0 < \lambda$ and the second inequality comes from the fact that since $0 < \lambda$ then $\mu c_n = e^T c_t$ which implies that $0 < c_t$.

Utilizing the inequalities from (13) we revisit (8) and write it with c_n, c_t and λ as variables:

$$\begin{bmatrix} J_n^T M^{-1} J_n & J_n^T M^{-1} J_t & 0 \\ J_t^T M^{-1} J_n & J_t^T M^{-1} J_t & 1 \\ \mu & -1 & 0 \end{bmatrix} \begin{bmatrix} c_n \\ c_t \\ \lambda \end{bmatrix} = - \begin{bmatrix} J_n^T b \\ J_t^T b \\ 0 \end{bmatrix} \tag{14}$$

where:

$$b = v_k + hM^{-1}(-\nabla V - k(q,v) + F_{ext}) \tag{15}$$

$$M^{-1} = \text{diag}\{\frac{1}{m}, \frac{1}{m}, \frac{1}{I}\}, \qquad \nabla V = \text{diag}\{0, mg, 0\}, \qquad F_{ext} = \begin{bmatrix} F_x & F_y & \tau \end{bmatrix}^T$$

$$\tilde{\omega} = \begin{bmatrix} 0 & -\dot{\theta} & 0 \\ \dot{\theta} & 0 & 0 \\ 0 & 0 & 0 \end{bmatrix}, \; R = \begin{bmatrix} \cos\theta & -\sin\theta & 0 \\ \sin\theta & \cos\theta & 0 \\ 0 & 0 & 1 \end{bmatrix}, \; k = \begin{bmatrix} 0 \\ 0 \\ \tilde{\omega} R I_0 R^T \omega \end{bmatrix} = \begin{bmatrix} 0 \\ 0 \\ 0 \end{bmatrix}$$

and we can solve for c_n and c_t to arrive at:

$$c_n = m \frac{\dot{y}_k + \theta_k J_{y,k} - hg + \frac{h}{m}(F_y + h\frac{m}{I}\tau)}{1 + \left(J_{y,k}^2 + \mu J_{x,k} J_{y,k}\right)\frac{m}{I}} = \frac{c_t}{\mu} \tag{16}$$

At this stage we have explicitly solved for the contact forces as functions of the inertial properties, geometry of contact and pre-contact kinematic measurements. To perform identifiability analysis we require an equation that is strictly a function of kinematic measurements and inertial properties so we replace the values derived for c_n and c_t into the equation of motion (3):

$$\begin{bmatrix} \dot{x}_{k+1} - \dot{x}_k \\ \dot{y}_{k+1} - \dot{y}_k + hg \\ \dot{\theta}_{k+1} - \dot{\theta}_k \end{bmatrix} = \frac{\dot{y}_k + \dot{\theta}_k J_{y,k} - hg + \frac{h}{m}(F_y + h\frac{m}{I}\tau)}{1 + \left(J_{y,k}^2 + \mu J_{x,k} J_{y,k}\right)\frac{m}{I}} \begin{bmatrix} \mu \\ 1 \\ \frac{m}{I}\left(J_{y,k} + \mu J_{x,k}\right) \end{bmatrix} + h \begin{bmatrix} \frac{F_x}{m} \\ \frac{F_y}{m} \\ \frac{\tau}{I} \end{bmatrix} \tag{17}$$

We can further manipulate (17) to yield the linear mapping:

$$Y = \Psi \Theta \tag{18}$$

where:

$$Y = \begin{bmatrix} \begin{bmatrix} \dot{x}_{k+1} - \dot{x}_k \\ \dot{y}_{k+1} - \dot{y}_k + hg \end{bmatrix} - \begin{bmatrix} \mu \\ 1 \end{bmatrix} \left(\dot{y}_k + \dot{\theta}_k J_y - hg\right) \\ \dot{\theta}_{k+1} - \dot{\theta}_k \end{bmatrix}$$

$$\psi_1 = \begin{bmatrix} hF_y\mu + hF_x \\ hF_y \\ 0 \end{bmatrix}, \qquad \psi_2 = \begin{bmatrix} hJ_y\tau \begin{bmatrix} \mu \\ 1 \end{bmatrix} + \left(J_{y,k}^2 + \mu J_{x,k} J_{y,k}\right) h \begin{bmatrix} F_x \\ F_y \end{bmatrix} \\ (J_y + \mu J_x)\, hF_y + h\tau \end{bmatrix} \tag{19}$$

$$\psi_3 = (J_y + \mu J_x) \begin{bmatrix} -J_y \begin{bmatrix} \dot{x}_{k+1} - \dot{x}_k \\ \dot{y}_{k+1} - \dot{y}_k + hg \end{bmatrix} \\ \dot{y}_k + \dot{\theta}_k J_y - hg - \left(\dot{\theta}_{k+1} - \dot{\theta}_k\right) J_y \end{bmatrix}, \qquad \psi_4 = \begin{bmatrix} 0 \\ 0 \\ (J_y - \mu J_x)\, hJ_y\tau \end{bmatrix}$$

$$\Psi = \begin{bmatrix} \psi_1 & \psi_2 & \psi_3 & \psi_4 \end{bmatrix}$$

$$\Theta = \begin{bmatrix} \frac{1}{m} & \frac{1}{I} & \frac{m}{I} & \frac{m}{I^2} \end{bmatrix}^T$$

Equation (18) is linear in the inertial parameters and assuming that Θ is the unknown vector of inertial parameters then, given samples of Y and Ψ, we can set up a constrained least squares estimation problem to determine m and I. Furthermore with the mass and moment of inertia identified we can infer the contact forces from (16), and conclude that the uniquely identifiable set is $\{m, I, c_n, c_t\}$. Assuming externalforces (excluding gravity) are set to zero then $\psi_1 = 0$, $\psi_2 = 0$ and $\psi_4 = 0$ which means that the only identifiable parameter is m/I. Replacing the value of m/I into (16) we can find c_t/m and c_n/m therefore the set of parameters that we can estimate uniquely in this case is $\{m/I, c_t/m, c_n/m\}$.

4.2 Sticking Contact Mode

During sticking contact the complementarity constraints in (8) become:

$$0 < c_n, \qquad 0 < c_t, \qquad \lambda = 0 \tag{20}$$

The first inequality is direct consequence of being in contact, as in the previous case. Since we are in sticking contact then a tangential force must exist to prevent sliding, therefore c_t must be greater than zero. A less intuitive justification can be garnered by considering the complementarity constraints of (8) and noting that since the velocity post contact will not have a component within the tangential plane of contact then $D^T v_{k+1} = 0$. In this scenario either $e^T c_t = \mu c_n$ which implies that frictional force is at its boundary and the analysis will follow as in Section 4.1 or that $e^T c_t \leq \mu c_n$ which implies that the frictional force lies inside the friction cone. Note that simply requiring that $D^T v_{k+1} = 0$ will result in $\lambda = 0$. Where the frictional force lies inside the boundary of its maximum, the LCP formulation from (8) simplifies to:

$$\begin{bmatrix} J_n^T M^{-1} J_n & J_n^T M^{-1} J_t \\ J_t^T M^{-1} J_n & J_t^T M^{-1} J_t \end{bmatrix} \begin{bmatrix} c_n \\ c_t \end{bmatrix} + \begin{bmatrix} J_n^T b \\ J_t^T b \end{bmatrix} = 0 \tag{21}$$

We solve for c_n and c_t and replace expressions from (15):

$$\begin{bmatrix} c_n \\ c_t \end{bmatrix} = \frac{-m}{1+\frac{m}{I}\left(J_y^2+J_x^2\right)} \begin{bmatrix} 1+\frac{m}{I}J_x^2 & -\frac{m}{I}J_xJ_y \\ -\frac{m}{I}J_xJ_y & 1+\frac{m}{I}J_y^2 \end{bmatrix} \begin{bmatrix} \dot{y}_k - hg + \dot{\theta}_k J_y + \frac{h}{m}(F_y + \frac{m}{I}\tau J_y) \\ \dot{x}_k + \dot{\theta}_k J_x + \frac{h}{m}(F_x + \frac{m}{I}\tau J_x) \end{bmatrix} \tag{22}$$

Replacing the expressions for contact forces into the equation of motion (3), and rearranging we have:

$$Y = \begin{bmatrix} \dot{x}_{k+1} + \dot{\theta}_k J_x \\ \dot{y}_{k+1} + \dot{\theta}_k J_y \\ \dot{\theta}_{k+1} - \dot{\theta}_k \end{bmatrix}, \qquad \psi_1 = \begin{bmatrix} -\left(J_y^2+J_x^2\right)\dot{x}_{k+1} + J_x^2\dot{x}_k + J_xJ_y\left(\dot{y}_k - hg\right) \\ -\left(J_y^2+J_x^2\right)\dot{y}_{k+1} + J_xJ_y\dot{x}_k + J_y^2\left(\dot{y}_k - hg\right) \\ -\left(J_y^2+J_x^2\right)\dot{\theta}_{k+1} - J_x\dot{x}_k - J_y\left(\dot{y}_k - hg\right) \end{bmatrix}$$

$$\psi_2 = h\begin{bmatrix} -F_xJ_y^2 + F_yJ_xJ_y - J_x\tau \\ F_xJ_xJ_y - J_x^2F_y - J_y\tau \\ -F_xJ_x - F_yJ_y + \tau \end{bmatrix}, \quad \psi_3 = \begin{bmatrix} 0 \\ 0 \\ -(J_x^2+J_y^2)h\tau \end{bmatrix}, \quad \psi_4 = h\begin{bmatrix} F_x \\ F_y \\ 0 \end{bmatrix}$$

$$\Theta = \begin{bmatrix} \frac{m}{I} & \frac{1}{I} & \frac{m}{I^2} & \frac{1}{m} \end{bmatrix}^T, \qquad \Psi = \begin{bmatrix} \psi_1 & \psi_2 & \psi_3 & \psi_4 \end{bmatrix} \tag{23}$$

By careful inspection we conclude that the inertial parameters m and I are uniquely identifiable in the presence of known external forces (excluding gravity) and we can infer contact forces from (22). Furthermore, if external forces are non-existent then $\psi_2 = \psi_3 = \psi_4 = 0$ and in this case only the ratio of mass to second moment of inertia and the ratio of contact forces to the mass of the object are identifiable. These results are consistent with sliding contact mode.

5 Examples: Block and Ellipse

In this section we apply the identifiability analysis in Section 4.1 and Section 4.2 to two examples: 2-D block and 2-D ellipse undergoing free-fall and colliding with a fix flat surface perpendicular to the direction gravity. We use two data sets validating the derivations: i) simulated data using a numerical implementation of time-stepping LCP and ii) experimental data recorded with a high speed camera. In both scenarios we measure the position, orientation and velocities of the bodies as they interact with the environment and attempt to identify the inertial parameters.

5.1 Identification Formulation

We consider a rigid body as in Fig. 2 at contact, denoting pre-impact time step as k and post impact time step as $k+1$:

$$\begin{bmatrix} \dot{x}_{k+1} \\ \dot{y}_{k+1} \\ \dot{\theta}_{k+1} \end{bmatrix} = \begin{bmatrix} \dot{x}_k \\ \dot{y}_k \\ \dot{\theta}_k \end{bmatrix} + h\begin{bmatrix} 0 \\ -g \\ 0 \end{bmatrix} + \frac{c_n}{m}\begin{bmatrix} 0 \\ 1 \\ \frac{m}{I}J_y \end{bmatrix} + \frac{c_t}{m}\begin{bmatrix} 1 \\ 0 \\ \frac{m}{I}J_x \end{bmatrix} \tag{24}$$

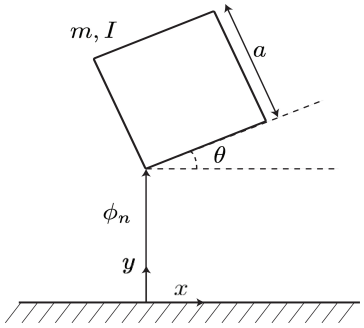

Fig. 3: 2D Block in Free-Fall

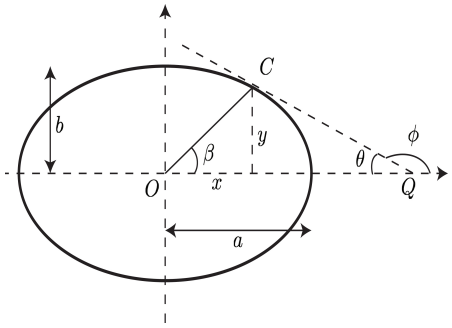

Fig. 4: 2D Ellipse Schematic

Since we are interested in the inertial parameters and assume that no known external forces (except gravity) act on the object during contact, from our analysis we can identify m/I. With this in mind a simple manipulation of (24) yields the least squares optimization problem:

$$\min_x ||Y - Ax||_2 \tag{25}$$

$$\text{where:} \quad Y = \dot{\theta}_{k+1} - \dot{\theta}_k, \quad A = (\dot{x}_{k+1} - \dot{x}_k)J_x - (\dot{y}_{k+1} - \dot{y}_k + hg)J_y, \quad x = \frac{m}{I}$$

The solution of (25) yields an estimate of m/I. So far we have been agnostic to the shape of the rigid body, we note that the shape of the object will affect the choice of the contact Jacobian and will be case specific, in the subsequent sections we derive expressions for the contact Jacobians of the block and ellipse.

5.1.1 2D Block

The block (Fig. 3) is modeled as a 2D square with length a, angle of rotation θ, center of mass at location (x,y), mass m and second moment of inertia I. We define the distance of the lowest vertex to the ground as a function of the configuration of the block:

$$\phi_n = \min\left(\begin{bmatrix} f_1(q) = y - \frac{a}{\sqrt{2}}\cos(\pi/4 - \theta) \\ f_2(q) = y - \frac{a}{\sqrt{2}}\cos(\pi/4 + \theta) \\ f_3(q) = y + \frac{a}{\sqrt{2}}\cos(\pi/4 - \theta) \\ f_4(q) = y + \frac{a}{\sqrt{2}}\cos(\pi/4 + \theta) \end{bmatrix}\right) \tag{26}$$

where $f_i(q)$ denotes the vertical distance of vertex i to the ground as a function of the height of the center of mass of the block y and it orientation θ.

We derive the contact Jacobians by differentiating (12). We assume that the lowest vertex is $f_1(q)$ and that we observe a single point contact, i.e., curvature does not play a role, which means that $\frac{\partial \beta}{\partial \theta} = 0$. Invoking (12) with this constraint and noting

that $\beta = \pi/4$ and $l = a/\sqrt{2}$ for vertex 1, the normal and tangential Jacobians are:

$$J_n = \begin{bmatrix} 0 & 1 & -\frac{a}{\sqrt{2}}\sin(\pi/4-\theta) \end{bmatrix}^T, \qquad J_t = \begin{bmatrix} 1 & 0 & \frac{a}{\sqrt{2}}\cos(\pi/4-\theta) \end{bmatrix}^T \tag{27}$$

Note that for a simple case such as the square, we could arrive at the same expression for the contact Jacobians simply by taking the partials of the contact constraints with respect to the configurations:

$$h(q) = \begin{bmatrix} y - \frac{a}{\sqrt{2}}\cos(\pi/4-\theta) \\ x - \frac{a}{\sqrt{2}}\sin(\pi/4-\theta) \end{bmatrix}, \qquad J_n = \frac{\partial h_1(q)}{\partial q}, \qquad J_t = \frac{\partial h_2(q)}{\partial q} \tag{28}$$

5.1.2 2D Ellipse

The ellipse, depicted in Fig. 4, is geometrically interesting because of the relative curvature between the surfaces in contact. Unlike the block, contact dynamics are very sensitive to orientation. Small perturbations of the object's orientation when in contact produces small changes to the contact location. We parametrize the perimeter curve of the ellipse by angle β, denote the major and minor radii of the ellipse with a and b, and refer to the contact point by C. The angle θ denotes the orientation of the ellipse with respect to line QC which for our purpose is the surface of contact. To compute the Jacobian from (12) we use geometry to relate β and θ:

$$\tan(\pi-\theta) = -\frac{b}{a}\cot\beta \xrightarrow{\frac{\partial}{\partial\theta}} \frac{\partial\beta}{\partial\theta} = -\frac{a}{b}\frac{1+\tan^2(\pi-\theta)}{1+\cot^2(\beta)} \tag{29}$$

We can write the distance of any point on the perimeter of an ellipse from its center as:

$$l(\beta) = \frac{ab}{\sqrt{b^2\cos^2\beta + a^2\sin^2\beta}} \xrightarrow{\frac{\partial l}{\partial\theta}} \frac{\partial l}{\partial\theta} = \frac{ab(b^2-a^2)\sin 2\beta}{2\sqrt{(b^2\cos^2\beta + a^2\sin^2\beta)^3}}\frac{\partial\beta}{\partial\theta} \tag{30}$$

Which allows us to find the expression for $\partial l/\partial\theta$. With these expressions we can can complete the optimization of (25).

5.2 Results from Simulated Data

To demonstrate the identification procedure we implemented a time-stepping LCP script to simulate a block and an ellipse with unit mass (kg), coefficient of restitution of 0.6 bouncing on a flat rigid fixed surface that lies perpendicular to the direction of the gravitational field and has 0.7 coefficient of friction. The ratio of mass to second moment of inertia for the block and ellipse are 6 (m^2) and 0.8 (m^2) respectively. To

generate data, both bodies were given a random set of initial positions and velocities and the simulation was run 100 times. Traces of example trajectories for the block and ellipse are shown in Fig. 5 and Fig. 6.

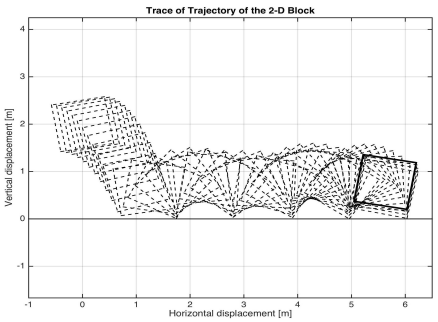

Fig. 5: 2D Block Trace

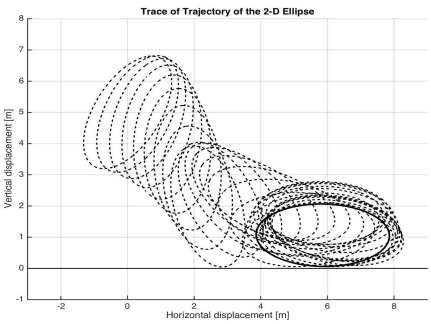

Fig. 6: 2D Ellipse Trace

We added gaussian noise $\sim \mathcal{N}(0, \sigma^2)$ to the simulated data collected (configurations and velocities) where σ is a function of signal to noise ratio. We then used the resulted signals to to calculate m/J following the least squares formulation in (25).

Table 1 shows the numerical results of the optimization as a function of signal to noise ratio where the first column denotes the mean error between predicted and actual m/J value, the second column denotes the percent error and the final column denotes the magnitude of the noise on measurements. We see good agreement between the predicted and true parameter with low levels of noise and a steady deterioration of prediction as noise is increased. We attribute the increasing error mostly to the contact Jacobians. Poor evaluation of these variables results in poor behavior prediction, which makes it difficult to estimate parameters.

Table 1: 2D Block Numerical Simulation and Identification Results

Block		Ellipse		Noise
Mean Error (m^2) $\pm$ Std.	% Error	Mean Error (m^2) $\pm$ Std.	% Error	S.N.R. (dB)
-0.021 $\pm$ 0.097	-0.35	-0.031 $\pm$ 0.101	-0.31	40
-0.125 $\pm$ 0.311	-2.083	-0.136 $\pm$ 0.443	-2.34	30
-0.659 $\pm$ 0.912	-10.98	-0.712 $\pm$ 0.820	-11.71	20
-3.491 $\pm$ 1.366	-58.197	-4.891 $\pm$ 1.938	-80.44	10

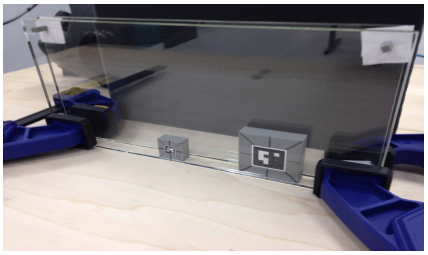

Fig. 7: Experimental Setup

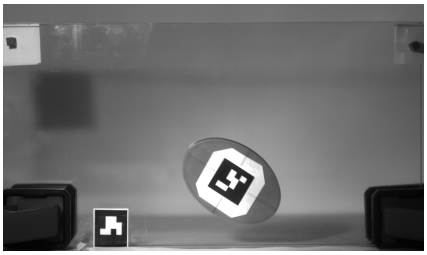

Fig. 8: Frame from Ellipse Drop

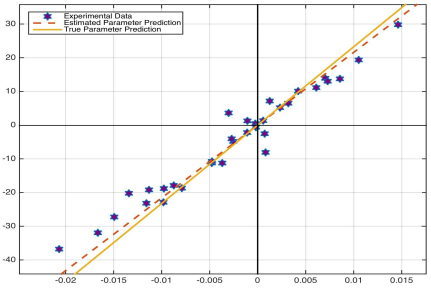

Fig. 9: Regression Results: Block, horizontal axes: A vertical axes: Y

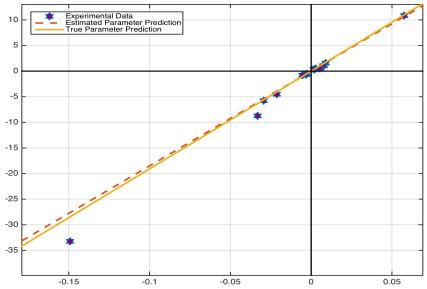

Fig. 10: Regression Results: Ellipse, horizontal axes: A vertical axes: Y

5.3 Results from Experimental Data

To further validate the identifiability analysis we constructed the experimental setup in Fig. 7. We used two flat sheets of glass with support spacers to constraint in the plane the motion of a falling object. For objects we used a 3D printed square of 2in side and an ellipse with major and minor radii of 1.5in and 1in. For observing the motion objects we used AprilTags [14] and a Fastec TS3 (Fastec Imaging Corp, San Diego, CA) high speed camera recording at 500 fps, which proved relatively sufficient to extract positions and orientations of the objects and velocity estimates by low-pass filtering and differentiation. For each drop experiment we considered the first 3 bounces and, and using the recovered configurations and velocities we evaluated the contact Jacobians and formed the optimization in (25).

Fig. 9 and Fig. 10 show the regression results from the data collected. We note the very good agreement between the identified and true inertial parameter m/I. Part of the discrepancies can be attributed to small errors due to friction and jittering of the objects as they slide over the glass and small deformations during contact. The glass and the gap between were chosen to minimize friction and undesired motions such as rotations out of plane, but small disturbances are difficult to prevent. The deformations at contact were very small due to the rigidity of the objects but small amounts of deformation may mean inaccuracies in the actual contact Jacobian and can influence identification.

6 Conclusions and Future Work

In this paper we investigated the problem of identifiability of inertial parameters and contact forces for a rigid body as it interacts with the environment through contact. The problem was broken down into the scenarios of sticking and sliding contact, with and without the presence of known external forces acting on the body (other than gravity). We showed that given a time history of the kinematic measurements of the object, i.e. its positions, orientations and derivatives of these quantities, without external force the parameters identifiable are the ratio of mass moment of inertia to mass of the object, and the ratio of the tangential and normal forces to mass. We also demonstrated that a known external force (other than gravity) acting on the object during the contact phase, can help in decouple the mass and mass moment of inertia, as well as the tangential and normal forces.

We validated the identifiability analysis on two planar free-falling rigid bodies undergoing frictional impact with the environment and showed that the results proved to be consistent with the predictions made by the identifiability analysis. The analysis was performed under assumptions which constitute the limitations of the work and serve as possible motivation for future efforts in this type of analysis. Future work could address issues such as increasing the number of simultaneous contacts, the number of rigid bodies, articulated rigid bodies, and extending the formulation to incorporate uncertainties in geometry.

References

[1] Anitescu M, Potra FA (1997) Formulating Dynamic Multi-Rigid-Body Contact Problems with Friction as Solvable Linear Complementarity Problems. Nonlinear Dynamics 14(3):231–247

[2] Anitescu M, Potra FA (2002) A time-stepping method for stiff multibody dynamics with contact and friction. International Journal for Numerical Methods in Engineering 55(7):753–784

[3] Atkeson CG (2012) State estimation of a walking humanoid robot. In: 2012 IEEE/RSJ International Conference on Intelligent Robots and Systems, IEEE, pp 3693–3699

[4] Brogliato B, ten Dam A, Paoli L, Génot F, Abadie M (2002) Numerical simulation of finite dimensional multibody nonsmooth mechanical systems. Applied Mechanics Reviews 55(2):107

[5] Chavan Dafle N, Rodriguez A (2015) Prehensile Pushing: In-hand Manipulation with Push-Primitives. In: IEEE/RSJ International Conference on Intelligent Robots and Systems (IROS), p To appear, URL http://hdl.handle.net/1721.1/98114

[6] Erdmann M (1998) Observing pose and motion through contact. In: Proceedings. IEEE International Conference on Robotics and Automation, IEEE, vol 1, pp 723–729
[7] Gautier M, Khalil W (1988) On the identification of the inertial parameters of robots. In: Proceedings of the 27th IEEE Conference on Decision and Control, IEEE, pp 2264–2269
[8] Khosla P, Kanade T (1985) Parameter identification of robot dynamics. In: 24th IEEE Conference on Decision and Control, IEEE, pp 1754–1760
[9] Koval MC, Dogar MR, Pollard NS, Srinivasa SS (2013) Pose estimation for contact manipulation with manifold particle filters. In: IEEE/RSJ International Conference on Intelligent Robots and Systems, IEEE, pp 4541–4548
[10] Lynch KM, Mason MT (1996) Stable Pushing: Mechanics, Controllability, and Planning. The International Journal of Robotics Research 15(6):533–556
[11] Müller P, Pöschel T (2011) Two-ball problem revisited: limitations of event-driven modeling. Physical review E, Statistical, nonlinear, and soft matter physics 83(4 Pt 1):041,304
[12] Platt R, Kaelbling L (2011) Efficient planning in non-gaussian belief spaces and its application to robot grasping. ... Symposium on Robotics ...
[13] Posa M, Cantu C, Tedrake R (2013) A direct method for trajectory optimization of rigid bodies through contact. The International Journal of Robotics Research 33(1):69–81
[14] Richardson A, Johannes S, Olson E (2011) AprilTag: A robust and flexible visual fiducial system. Proceedings of the IEEE International Conference on Robotics and Automation (ICRA) (3400-3407)
[15] Rodriguez A, Bourne D, Mason M, Rossano GF (2010) Failure detection in assembly: Force signature analysis. In: IEEE International Conference on Automation Science and Engineering, IEEE, pp 210–215
[16] Salawu O (1997) Detection of structural damage through changes in frequency: a review. Engineering Structures 19(9):718–723
[17] Slotine JJE (1987) On the Adaptive Control of Robot Manipulators. The International Journal of Robotics Research 6(3):49–59
[18] Stewart D, Trinkle JC (1996) An Implicit Time-Stepping Scheme for Rigid Body Dynamics with Inelastic Collisions and Coulomb Friction. International Journal for Numerical Methods in Engineering 39(15):2673–2691
[19] Stewart DE (2000) Rigid-Body Dynamics with Friction and Impact. SIAM Review 42(1):3–39
[20] Trinkle J (2013) A dynamic Bayesian approach to real-time estimation and filtering in grasp acquisition. In: IEEE International Conference on Robotics and Automation, IEEE, pp 85–92
[21] Yu KT, Leonard J, Rodriguez A (2015) Shape and Pose Recovery from Planar Pushing. In: IEEE/RSJ International Conference on Intelligent Robots and Systems (IROS), p To appear, URL http://hdl.handle.net/1721.1/100413
[22] Zhang L, Trinkle JC (2012) The application of particle filtering to grasping acquisition with visual occlusion and tactile sensing. In: IEEE International Conference on Robotics and Automation, IEEE, pp 3805–3812